Tidal Waves in ^{102}Pd: A Rotating Condensate of Multiple d Bosons

A. D. Ayangeakaa,[1] U. Garg,[1] M. A. Caprio,[1] M. P. Carpenter,[2] S. S. Ghugre,[3] R. V. F. Janssens,[2] F. G. Kondev,[4]
J. T. Matta,[1] S. Mukhopadhyay,[5,*] D. Patel,[1] D. Seweryniak,[2] J. Sun,[1] S. Zhu,[2] and S. Frauendorf[1]

[1]*Department of Physics, University of Notre Dame, Notre Dame, Indiana 46556, USA*
[2]*Physics Division, Argonne National Laboratory, Argonne, Illinois 60439, USA*
[3]*UGC-DAE Consortium for Scientific Research, Kolkata Centre, Kolkata 700 098, India*
[4]*Nuclear Engineering Division, Argonne National Laboratory, Argonne, Illinois 60439, USA*
[5]*Department of Physics, Mississippi State University, Mississippi State, Mississippi 39762, USA*
(Received 9 January 2013; published 5 March 2013)

Low-lying collective excitations in even-even vibrational and transitional nuclei may be described semiclassically as quadrupole running waves on the surface of the nucleus ("tidal waves"), and the observed vibrational-rotational behavior can be thought of as resulting from a rotating condensate of interacting d bosons. These concepts have been investigated by measuring lifetimes of the levels in the yrast band of the ^{102}Pd nucleus with the Doppler shift attenuation method. The extracted $B(E2)$ reduced transition probabilities for the yrast band display a monotonic increase with spin, in agreement with the interpretation based on rotation-induced condensation of aligned d bosons.

Collective quadrupole excitations of nuclei are classified as "rotational" and "vibrational" with the rigid rotor and the harmonic vibrator being the limiting ideal cases. The harmonic vibrations (d bosons) are fivefold degenerate with respect to the angular momentum projection; they couple to multiplets of different angular momentum. Rotational bands that extend over ten or more states are ubiquitous. Vibrational excitations of spherical nuclei, on the other hand, are much less distinct since the time scale of collective vibrations is not much larger than that of intrinsic quasiparticle excitations. The adiabatic separation of the time scales, which is a prerequisite for the appearance of collective quantum states, rapidly deteriorates with the number of excited quanta (phonons). While evidence for the two-phonon triplet is often observed, identification of all members of the three-phonon multiplet is already problematic (see, for example, Ref. [1]). Figure 1 schematically shows the location of the vibrational states and of the quasiparticle excitations for a spherical nucleus. With increasing phonon number n, the collective states are embedded into a progressively dense background of quasiparticle excitations. The coupling to this quasiparticle background fragments the collective levels and they cease to exist as individual quantum states. The density of quasiparticle excitations is lowest near the yrast line, which is the sequence of states with the lowest excitation energy for a given angular momentum I. With increasing phonon number n, the yrast members of the vibrational multiplets are expected to keep their identity as collective quantum states the longest.

In this Letter, we report on the first identification of a seven-phonon yrast state, which can be interpreted as a rotating condensate of seven d bosons that align their spins. The yrast states of ^{102}Pd are nearly equidistant in energy up

to spin $I = 16$, which is characteristic of a vibrational sequence. Indeed, the existence of an exceptionally long vibrational band in ^{102}Pd was already noted by Regan *et al.* [2], making this nucleus an attractive case for this investigation. However, in order for these states to represent a sequence of stacked d bosons, the reduced transition probabilities between adjacent states, $B(E2; I \rightarrow I - 2)$, must increase linearly with the number of bosons. In this work, lifetime measurements are presented that confirm this expectation. The measurements are complemented by theory, which provides a connection with the underlying microscopic structure that has remained a challenge in the case of multiphonon excitations.
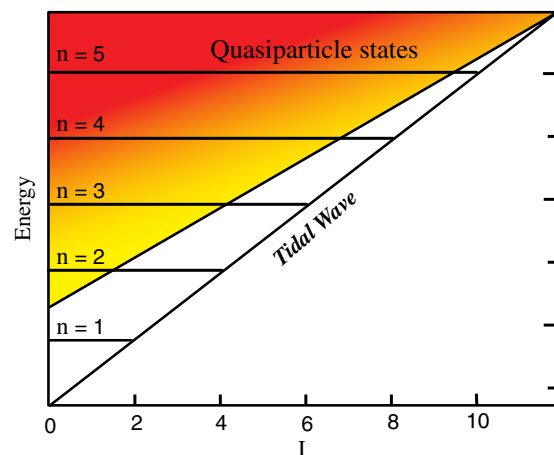

FIG. 1 (color online).   Schematic representation of the location of the collective quadrupole vibrational excitations relative to the quasiparticle excitations. The darker shades approximately indicate higher densities of quasiparticle states.

Figure 2 illustrates the vibrational modes of minimal and maximal angular momentum of a classical ideal liquid. The oscillating standing wave on the left-hand side represents the zero-angular momentum members of the vibrational multiplets, which are most rapidly drowned in the sea of quasiparticle excitations. The vibrational yrast states correspond to a wave traveling over the nuclear surface, as illustrated on the right-hand side. The surface rotates with the constant angular velocity ω as is the case for the rotation of a rigid body. However, the flow pattern is irrotational. As is characteristic of a surface wave, liquid moves from the wave front under the crest to the back side. The energy and the angular momentum increase with the amplitude of the wave, but the frequency remains constant. In the case of rigid rotation, the energy and the angular momentum increase with the angular frequency while the shape remains unchanged. The name "tidal wave" has been suggested for the yrast mode [3] in analogy to the propagation of ocean tidal waves. The tidal wave then corresponds to a wave packet of aligned d bosons, which rotates with constant angular velocity. The tidal wave concept has been applied previously to near-equidistant band structures of different spin-parity sequences. Specifically, Refs. [4,5] interpreted the $\Delta I = 1$ sequences of fixed parity in ^{182}Os as a tidal wave running over a triaxial surface, and Ref. [6] interpreted the alternating-parity sequences in ^{220}Th as a reflection-asymmetric tidal wave traveling over a spherical core.

In terms of a rotational interpretation, the difference between a rotor and a tidal wave lies in the way in which angular momentum is generated. A rotor generates angular momentum by increasing the angular frequency ω at nearly constant deformation (and, hence, constant moment of inertia). A tidal wave nucleus, on the other hand, generates angular momentum by increasing deformation (i.e., changing β, γ) at nearly constant angular frequency ω. For most transitional nuclei, the situation is intermediate: Both mechanisms of generating angular momentum are present, one favored over the other as the angular momentum increases. The rotorlike scenario has been well studied, with the measured reduced transition probabilities, i.e., $B(E2)$ values, confirming that the deformation remains rather constant [7]. However, the strong increase of deformation with angular momentum, which characterizes a tidal wave, is demonstrated for the first time in the work reported here.

The mean lifetimes of yrast states in ^{102}Pd were measured using the Doppler shift attenuation method (DSAM). The experiment was performed at the Argonne Tandem Linear Accelerator System facility using the ^{76}Ge(^{30}Si, $4n$) reaction, at a beam energy of 90 MeV. The target consisted of 500 μg/cm^2 isotopically enriched ^{76}Ge backed by a 26 mg/cm^2-thick layer of Au; the backing thickness was sufficient to stop the recoiling nuclei. A thin layer of 11 μg/cm^2 Al was sandwiched between the target and backing to prevent the migration of Ge into Au. The emitted γ rays were detected with the Gammasphere array [8] which, at the time of the experiment, comprised 98 Compton-suppressed high-purity Ge detectors, arranged in 16 rings of constant angles relative to the beam direction; a total of 3.1×10^9 three- and higher-fold coincidence events were accumulated. The low-spin structure of ^{102}Pd is already well established [9–11]. The present investigation has focused primarily on the measurement of the lifetimes of members of the yrast band.

The accumulated data were sorted angle-by-angle into several unique-fold event databases, using the BLUE program [12]. For each database, an angle-dependent background subtraction algorithm [13] was applied, and the resulting, background-subtracted, databases were double gated in order to extract coincidence and error spectra for each ring of Gammasphere for further analysis.

Doppler-shifted and broadened line shapes were observed for transitions in the yrast band up to the 16^+, 7244-keV level and lifetime analyses were performed using a modified version of the LINESHAPE analysis package [14]. A total of 50 000 Monte Carlo simulations of the velocity histories of the recoiling nuclei traversing the target and backing materials were generated in time steps of 0.0089 ps and were subsequently converted into time-dependent velocity profiles. The total number of time steps was set to 198 and the time step value was determined in accordance with the discussion in Ref. [14]. Electronic stopping powers were taken from Ziegler's tabulation [15] with low-energy modifications. Energies of in-band transitions were determined from fits to the experimental data and the side-feeding intensities obtained directly from the measured γ-ray intensities within the yrast band. The side feeding into each level and to the top of the yrast band
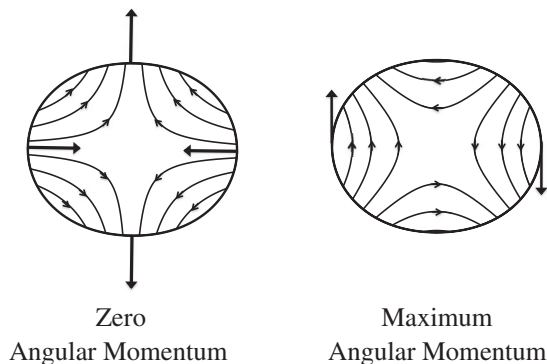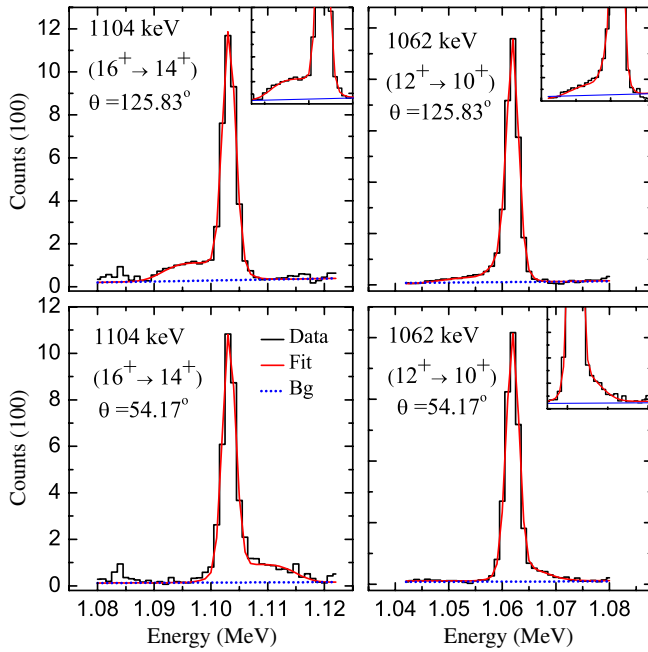

FIG. 2. Flow pattern of a vibrating droplet of an ideal liquid. The arrows indicate the motion of the surface. For a given energy, there are degenerate modes, which differ by their angular momentum. Left: The oscillating motion, which carries no angular momentum. Right: The traveling wave (tidal wave), which carries the maximal angular momentum (yrast state). The outward motion of the surface at the southeast and the inward motion at northeast combine such that the eastern crest moves down.

FIG. 3 (color online).   Line shape fits to the 1104- and 1062-keV transitions in the yrast band in ^{102}Pd. The upper and lower panels correspond to the backward and forward detectors, respectively. The inserts are expanded views of the line shapes.

TABLE I.   Measured lifetimes and electromagnetic transition probabilities for the yrast band in ^{102}Pd. Experimental uncertainties were derived from the behavior of χ^2 in the vicinity of the best-fit parameter values.

E_γ (MeV)	$I_i^\pi \rightarrow I_f^\pi$	τ (ps)	$B(E2)$ (e^2b^2)	Q_t (eb)
0.836	$6^+ \rightarrow 4^+$	1.149(32)	0.174(22)	2.36(15)
0.902	$8^+ \rightarrow 6^+$	0.720(42)	0.190(11)	2.41(07)
0.980	$10^+ \rightarrow 8^+$	0.409(28)	0.221(15)	2.56(09)
1.062	$12^+ \rightarrow 10^+$	0.252(18)	0.240(14)	2.65(08)
1.083	$14^+ \rightarrow 12^+$	0.201(11)	0.272(15)	2.80(08)
1.104	$16^+ \rightarrow 14^+$	0.180(21)[a]	0.277(14)	2.81(07)

[a]The lifetime of the 16^+ level could not be separated from the side-feeding lifetime. The value given is, therefore, the lower limit.

Figure 4 provides the experimental moments of inertia $\mathcal{J} = I/\omega = 2I/[E(I) - E(I-2)]$ as a function of spin I. The harmonic limit for the free bosons is displayed by the dash-dotted line marked FB and corresponds to a constant ω equal to one half of the vibrational frequency Ω. The experimental $\mathcal{J}$ is a nearly linear function of I as indicated by the dash-dotted line marked IB (for interacting bosons). It deviates from FB by the small offset at $I = 0$, which is a measure of the anharmonicity. The angular momentum increases due to the increase of $\mathcal{J}$ while ω remains nearly constant.

The measured $B(E2)$ values (Fig. 5) increase linearly with I, such that the ratio $B(E2)/\mathcal{J}$ is constant within the experimental uncertainties (see the insert). This demonstrates that the angular momentum gain originates from the increase of the wave amplitude (deformation) while the rotational frequency does not increase significantly. This is
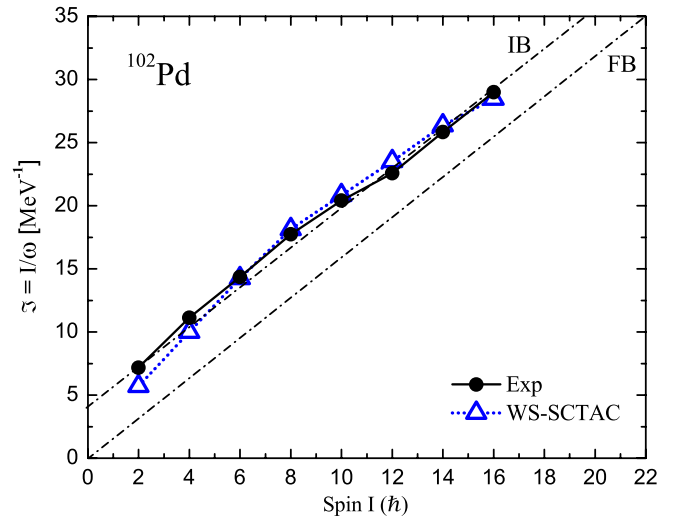
was modeled by a five-state rotational cascade with independently variable lifetimes. A χ^2 minimization for the observed Doppler shifted line shapes was then performed using the in-band and side-feeding lifetimes, background, and contaminant peak(s) as input parameters. Experimental uncertainties in the extracted lifetimes were determined based on the behavior of the χ^2 fit in the vicinity of the minimum [16,17] by a statistical method using the MINOS [18] program. Although side-feeding effects were initially included in the analysis, the extracted lifetimes were found to be insensitive to changes in the side-feeding intensities. More details on the fitting procedure can be found in Refs. [16,19].

Experimental data and line shape fits at both forward and backward angles for two representative transitions (1104 and 1062 keV) in the yrast band are displayed in Fig. 3. The inserts are expanded views of the corresponding line shapes. The extracted lifetimes of states in the yrast band, the corresponding reduced transition probabilities, and the associated transition quadrupole moments Q_t are summarized in Table I. The reduced transition probabilities were obtained from the measured lifetimes using the expression:

$$B(E2) = \frac{0.0816}{E_\gamma^5(E2)\tau(E2)} [e^2 b^2], \quad (1)$$

with the γ-ray energies, E_γ, in MeV, and the partial lifetimes of the transitions, $\tau(E2)$, in ps.

FIG. 4 (color online).   Moments of inertia, $\mathcal{J}$, as a function of spin, I. The dash-dotted line marked FB is the limit for harmonic bosons. The dash-dotted line marked IB indicates the near-linear trend of interacting bosons. WS-SCTAC represents the cranking + micro-macro calculations described in the text.
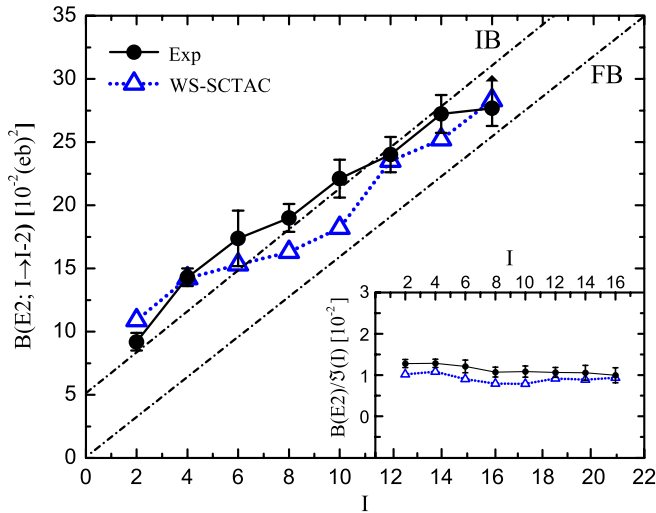
FIG. 5 (color online). Reduced electromagnetic transition
probabilities for the yrast states of ^{102}Pd as a function of the
spin, I. Lifetime data for the 2^+ and 4^+ states are from Ref. [23].
The dash-dotted line marked FB is the limit for harmonic
bosons. The dash-dotted line marked IB indicates the near-linear
trend of interacting bosons. WS-SCTAC represents the
cranking + micro-macro calculations described in the text. The
insert provides the experimental and calculated ratios $B(E2)/\mathcal{J}$
as a function of I.

in stark contrast to a typical rotor where the transition
probabilities remain relatively constant over a given spin
range, while the increase of the rotational frequency trans-
lates into a gain of angular momentum. This provides the
first evidence that the yrast line of ^{102}Pd corresponds to a
slightly anharmonic tidal wave and the measurements
reported here establish the characteristic increase of the
tidal wave amplitude up to $I = 14$.

It is remarkable that the anharmonicity shows up in a
simple way as a constant upshift of the functions $\mathcal{J}(I)$ and
$B(E2; I \rightarrow I - 2)$. This may be interpreted as follows: The
yrast line of ^{102}Pd is characterized by an anharmonic wave
that starts out with a small deformation (i.e., nonaligned d
bosons are present with a small probability) and increases
in amplitude along the sequence of states by adding aligned
d bosons.

The transition quadrupole moment measures the ampli-
tude of the tidal wave. For $^{102}_{46}$Pd$_{56}$, it is $Q_t = 2.8$ eb at
$I = 14$, to be compared with $Q_t = 2.96$ eb for the $I = 2$
state in the nucleus $^{110}_{46}$Pd$_{64}$, which is located in the middle
of the neutron shell [20]. In the case of ^{110}Cd, the experi-
mental amplitude of the tidal wave reaches $Q_t = 2.53$ eb
for $I = 8$ [20]. [All quoted Q_t values have been obtained
from the lifetime information provided in the cited refer-
ences.] In this case, the s configuration with the rotational
aligned pair of $h_{11/2}$ quasineutrons becomes yrast for
$I \geq 12$ [2]. Its nearly constant smaller deformation
($Q_t \sim 1.7$ eb) thereafter signals the transition to the
rotational regime (cf. Ref. [3]). In the case of ^{102}Pd, the

rotational aligned s configuration does not become yrast
until after $I = 16$, which, as mentioned previously, is one
reason why this nucleus was deemed very attractive from
the point of view of studying the boson condensate.
Unfortunately, it was not possible to determine the life-
times of these "rotational" states from the present data.

The tidal wave concept allows for a semiclassical cal-
culation of the energies and $B(E2)$ values of the yrast states
in vibrational and transitional nuclei. The tidal wave has a
static deformed shape in the corotating frame of reference.
This has led to the microscopic description suggested
in Ref. [3], which is based on the cranking model
without resorting to the small amplitude approximation.
Reference [3] applies the shell-correction tilted-axis crank-
ing (SCTAC) version [21] of the cranking model to even-
even nuclides with $44 \leq Z \leq 48$ and $56 \leq N \leq 66$. In this
approach, the energy surface is calculated by the micro-
macro method, subject to the constraint that the expecta-
tion value of the angular momentum operator equals I.
The energy is minimized with respect to the deformation
parameters β and γ. Deformed solutions are found in
Ref. [3] for $I \geq 2$, even when the solution was spherical
for $I = 0$. These calculations reproduce the collective yrast
states rather well. They also describe the intrusion of the
aligned $h_{11/2}$ two-quasineutron states into the yrast line,
which causes the backbending phenomenon seen in most
of the nuclei studied. The details of the present calculations
are the same as those of Ref. [3], with the exception that the
modified oscillator potential is replaced by a deformed
Woods-Saxon potential with the so-called "universal"
parameters [22]. The results are labeled by SCTAC in
Figs. 4 and 5 ("TAC" refers only to the code; the self-
consistent solution actually rotates about the intermediate
principal axis of the slightly triaxial shape). It should
be noted that there are no parameters adjusted to the
experiment.

As seen in Fig. 4, the observed behavior of $\mathcal{J}$ as a
function of spin I is reproduced well by these calculations.
The calculated $\mathcal{J}(I)$ moment remains close to the
IB line because the ground state configuration has been
employed throughout. The calculated $B(E2; I \rightarrow I - 2)$
values (Fig. 5) also follow the experimental data overall,
albeit with somewhat larger fluctuations than those exhib-
ited by the experimental values. The reason for this appar-
ent discrepancy lies in the fact that the deformation
parameters are those associated with the minimum of the
energy calculated by the micro-macro method. This method
neglects zero point fluctuations of the shape which,
when properly accounted for, are expected to result in
washing out of these fluctuations. Thus, the semiclassical
cranking + micro-macro calculations describe the yrast
states of ^{102}Pd up to the seven boson state rather well,
once the anharmonicities are correctly accounted for.

In summary, by measuring the lifetimes of the yrast
states in ^{102}Pd up to a spin of $I = 14$, the first clear

evidence has been provided for rotational-induced condensation of aligned d bosons. The linear increase of the reduced transition probability with the boson number $n = I/2$, which is expected for condensation, was observed up to $n = 7$. The mutual interaction of bosons causes anharmonicities which appear as a constant upshift of the reduced transition probability and the moment of inertia as a function of spin I. This upshift may be interpreted as caused by a small fraction of nonaligned d bosons to which the aligned d bosons are added. Semiclassically, the condensate represents a tidal wave traveling over the nuclear surface with constant angular velocity (equal to one half of the vibrational frequency), where the angular momentum gain arises from the increase of the wave amplitude. Since the wave motion is not quite harmonic, a slight increase of the rotational frequency with spin is seen. The tidal wave is described in the framework of the cranking model based on the micro-macro method, which describes the data well *without* any adjustment of the model parameters.

---

*Present address: Nuclear Physics Division, Bhabha Atomic Research Centre (BARC), Mumbai 400085, India.

[1] A. Aprahamian, D. S. Brenner, R. F. Casten, R. L. Gill, and A. Piotrowski, Phys. Rev. Lett. **59**, 535 (1987).

[2] P. H. Regan *et al.*, Phys. Rev. Lett. **90**, 152502 (2003).

[3] S. Frauendorf, Y. Gu, and J. Sun, Int. J. Mod. Phys. E **20**, 465 (2011).

[4] L. K. Pattison *et al.*, Phys. Rev. Lett. **91**, 182501 (2003).

[5] D. M. Cullen, R. Glover, L. K. Pattison, P. M. Walker, S. Frauendorf, and D. Almehed, J. Phys. G **31**, S1709 (2005).

[6] W. Reviol *et al.*, Phys. Rev. C **74**, 044305 (2006).

[7] B. Kotliński *et al.*, Nucl. Phys. **A517**, 365 (1990).

[8] I.-Y. Lee, Nucl. Phys. **A520**, c641 (1990).

[9] D. Jerrestam, W. Klamra, B. Fogelberg, R. Bark, A. Gizon, J. Gizon, E. Ideguchi, S. Mitarai, M. Piiparinen, and G. Sletten, Nucl. Phys. **A603**, 203 (1996).

[10] J. Gizon *et al.*, Phys. Lett. B **410**, 95 (1997).

[11] N. V. Zamfir *et al.*, Phys. Rev. C **65**, 044325 (2002).

[12] M. Cromaz, T. Symons, G. Lane, I. Lee, and R. MacLeod, Nucl. Instrum. Methods Phys. Res., Sect. A **462**, 519 (2001).

[13] K. Starosta, D. Fossan, T. Koike, C. Vaman, D. Radford, and C. Chiara, Nucl. Instrum. Methods Phys. Res., Sect. A **515**, 771 (2003).

[14] J. C. Wells and N. Johnson, Oak Ridge National Laboratory Report No. ORNL-6689, 1991, p. 44.

[15] J. Ziegler, in *Stopping and Ranges of Ions in Matter* (Pergamon Press, New York, 1980), Vols. 3 and 5.

[16] C. J. Chiara *et al.*, Phys. Rev. C **61**, 034318 (2000).

[17] U. Garg *et al.*, Phys. Lett. B **180**, 319 (1986).

[18] F. James and M. Roos, Comput. Phys. Commun. **10**, 343 (1975).

[19] C. J. Chiara *et al.*, Phys. Rev. C **64**, 054314 (2001).

[20] G. Gürdal and F. G. Kondev, Nucl. Data Sheets **113**, 1315 (2012).

[21] S. Frauendorf, Nucl. Phys. A **677**, 115 (2000).

[22] S. Cwiok, J. Dudek, W. Nazarewicz, J. Skalski, and T. Werner, Comput. Phys. Commun. **46**, 379 (1987).

[23] D. D. Frenne, Nucl. Data Sheets **110**, 1745 (2009).